Article **ECORFAN Journal-Democratic Republic of Congo**
December 2022, Vol.8 No.15 11-18

Rotor crack moment of inertia

Momento de inercia en fisura de rotor

JIMÉNEZ-RABIELA, Homero†*, VÁZQUEZ-GONZÁLEZ, Benjamín, RAMÍREZ-CRUZ, José Luis and ILIZALITURRI-BADILLO, Joshua Suraj

Universidad Autónoma Metropolitana, Unidad Azcapotzalco, División de Ciencias Básicas e Ingeniería, Departamento de Energía

ID 1st Author: *Homero, Jiménez-Rabiela* / **ORC ID** 0000-0002-1549-0853, **Researcher ID Thomson**: S-2299-2018, **CVU CONACYT ID**: 123386

ID 1st Co-author: *Benjamín, Vázquez-González* / **ORC ID**: 0000-0002-9030-5662, **Researcher ID Thomson**: S-2417-2018, **CVU CONACYT ID**: 25749

ID 2nd Co-author: *José Luis, Ramírez-Cruz* / **ORC ID**: 0000-0003-0762-2630, **Researcher ID Thomson**: G-3405-2019, **CVU CONACYT ID**: 921268

ID 3rd Co-author: *Joshua Suraj, Ilizaliturri-Badillo* / **ORC ID**: 0000-0003-2008-067X, **Researcher ID Thomson**: HGV-1387-2022

DOI: 10.35429/EJDRC.2022.15.8.11.18 Received July 20, 2022; Accepted December 30, 2022

Abstract

The objective of this article is to evaluate the change in the moment of inertia of a rotor with chordal diagonal triangular crack, in all cross sections from the beginning to the end of it. The triangle used to generate the crack is isosceles and its inclination with respect to the transversal will be constant and equal to one sixth of π. The quotient of the width between the depth of the crack, from its birth and during its growth, is invariant and equal to 0.2. The ratio of the depth of the crack between the radius will vary from 0.4 to 0.6. The moment of inertia of the resulting cross-sectional area is calculated from the moments of inertia of component areas. Since in the antecedents there is information about cracks: transverse chordal rectangular, diagonal chordal rectangular, transverse chordal triangular; the present work expands the knowledge of the moment of inertia of the cracks to those that are triangular diagonal chordal; increasing the evidence for the subsequent early detection of cracks in rotors.

Rotor, Cracks, Moment of inertia

Resumen

El objetivo del presente artículo es evaluar el cambio en el momento de inercia de un rotor con fisura triangular diagonal cordal, en todas las secciones transversales desde el inicio hasta el fin de ésta. El triángulo usado para generar la fisura es isósceles y su inclinación con respecto a la transversal será constante e igual a un sexto de π. El cociente del ancho entre la profundidad de la fisura, desde su nacimiento y durante su crecimiento, es invariante e igual a 0.2. El cociente de la profundidad de la fisura entre el radio será variable de 0.4 a 0.6. El momento de inercia del área transversal resultante se calcula a partir de los momentos de inercia de áreas componentes. Puesto que en los antecedentes se encuentra información sobre fisuras: rectangulares transversales cordales, rectangulares diagonales cordales, triangulares transversales cordales; el presente trabajo expande el conocimiento del momento de inercia de las fisuras a aquellas que son triangulares diagonales cordales; incrementando los elementos de juicio para la ulterior detección temprana de fisuras en rotores.

Rotores, Fisuras, Momento de inercia

Citation: JIMÉNEZ-RABIELA, Homero, VÁZQUEZ-GONZÁLEZ, Benjamín, RAMÍREZ-CRUZ, José Luis and ILIZALITURRI-BADILLO, Joshua Suraj. Rotor crack moment of inertia. ECORFAN Journal-Democratic Republic of Congo. 2022. 6-10:11-18.

* Correspondence to Author (E-mail: hjr@azc.uam.mx)
† Researcher contributing first author.

Introduction

The evaluation of the moment of inertia of rotors in the cross sections corresponding to their cracking is important as it allows the early detection of cracking. The interest of the scientific community in the subject is noted by the publication of articles related to the topic, some of which are described below: A. Lazarus, et al (2008), applying eigenvalues and eigenvectors, as well as Floquet's theory and Mathieu's equation, studied rotating systems and their asymmetric rigidity. Ramezanpour, et al (2012), investigated the behavior of a Jeffcott rotor with diagonal crack in arbitrary orientation, using fracture mechanics concepts they determined the stiffness and flexibility matrices of the system. Ghozlane, M. (2015), proposed a simplified approach to model an open crack in a rotor based on the change of its flexibility. Gou, G. & Liu, C. (2016), determined the stiffness variation of a rotor containing a transverse crack. Fellah, A., Jadjoui, A. & Bakhaled, B. (2017), studied the effect of a transverse crack in a rotor taking into account the stiffness variation. Bakhaled, B., Jadjoui, A. & Fellah, A. (2018), proposed a new method, based on the theory of local stiffness decrease in a cracked rotor, to predict the presence of a crack. Jameel, A. & Thijeel, J. (2019), estimated the effect of a crack on the critical rotor speed using two methods: analytical and fast Fourier transform. Joseph, S. Helen, W. & Richard, Y. (2020), applied non-symmetric bending principles in rotor crack modeling without assuming horizontality of the neutral plane. Peter, K. & Robert, G. (2021), presented two simple methods to measure the moment of inertia of rotors without disassembly and without special laboratory equipment. Mohammad, A. & Fatima, K. (2021). They introduce an effective stiffness measure to analyze the effect of crack and unbalance force vector orientation on the negative potential intensity. Mo, Y. Hao, X, & Wei, X. (2022), Established an improved stiffness model of composite shaft crack based on layer theory, which considered the influence of orientation angle and stacking sequence of cracked layers.

The present work has added value in that, to date, no exact expressions have been published to determine the moment of inertia in the chordal diagonal triangular crack of a rotor.

The moment of inertia of the rotor cross sections, in its cracked zone, is obtained considering the rotor static and with the center of gravity of the crack on the axis with respect to which the moment of inertia is evaluated.

The exact evaluation of the moment of inertia in the cracked area will subsequently allow to know the global stiffness of the rotor and to predict more accurately its useful life. The following premise is assumed: Every geometry, however complex it may be, is composed of basic geometries.

Units and nomenclature are defined in the first section. Geometric calculations are described in the second section. The component areas are described in the third section. The moment of inertia of the component areas is determined in the fourth section. In the fifth section the moment of inertia for the area of interest is obtained. The results and conclusions are expressed in the sixth and seventh sections, respectively.

Units and nomenclature

Lengths in millimeters and angles in radians

Figure 1 shows the invariant input parameters. L = rotor length between supports, r = rotor radius. The origin of the inertial reference frame is at the center of the rotor at its initial cross section. The crack center is 0.5L from the origin of coordinates.

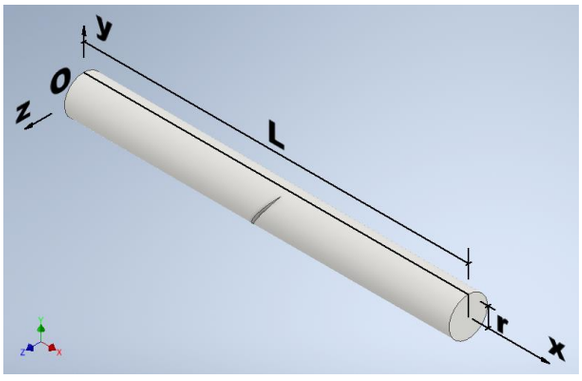

Figure 1 Cracked rotor
Source: Own elaboration

ISSN 2414-4924

In Figure 2 the shear plane is obtained by rotating the xz-plane an angle around an axis 0.5L from the z-axis. Figure 3 shows the linear variable input parameters: a = crack width, p = crack depth. A, B, C and D are material points of the tool (isosceles triangle) used to generate the crack. E and F are material points on the crack edges, their distances to the rotor center are equal to r.

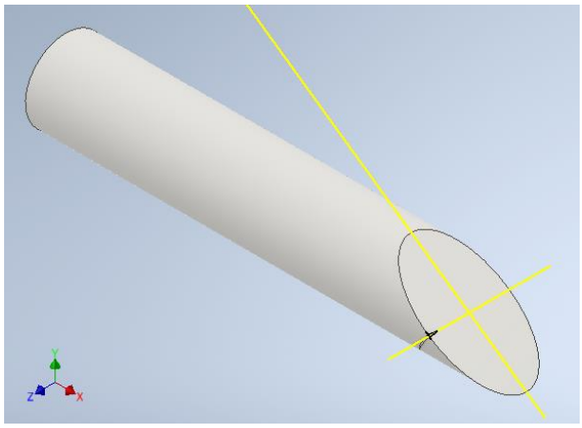

Figure 2 Diagonal cut
Source: Own elaboration

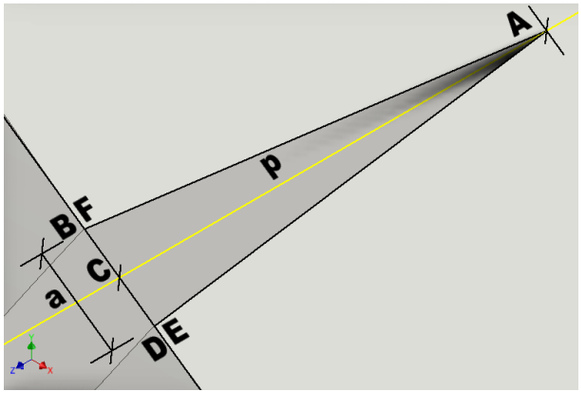

Figure 3 Detail of Figure 2
Source: Own elaboration

Geometric calculations

In Figure 4 the shear plane is obtained by moving the xy plane a distance equal to r-p in the positive direction of the z-axis. Figure 5 shows the ith point A, where i will vary from 0 to 500, at the bottom of the crack, and from it the following equations are inferred:

$$y_{max} = \sqrt{2rp - p^2} \quad (1)$$

$$c = y_{max} Tg(\alpha) \quad (2)$$

$$x_{A_0} = 0.5L - c \quad (3)$$

$$x_{A_i} = x_{A_0} + i\frac{2c}{n} \quad (4)$$

$$x_{A_n} = 0.5L + c \quad (5)$$

$$d = \frac{x_{A_i} - x_{A_0}}{Tg(\alpha)} \quad (6)$$

$$y_{A_i} = d - y_{max} \quad (7)$$

$$z_{A_i} = r - p \quad (8)$$

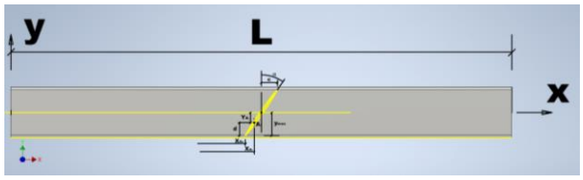

Figure 4 Crack front view
Source: Own elaboration

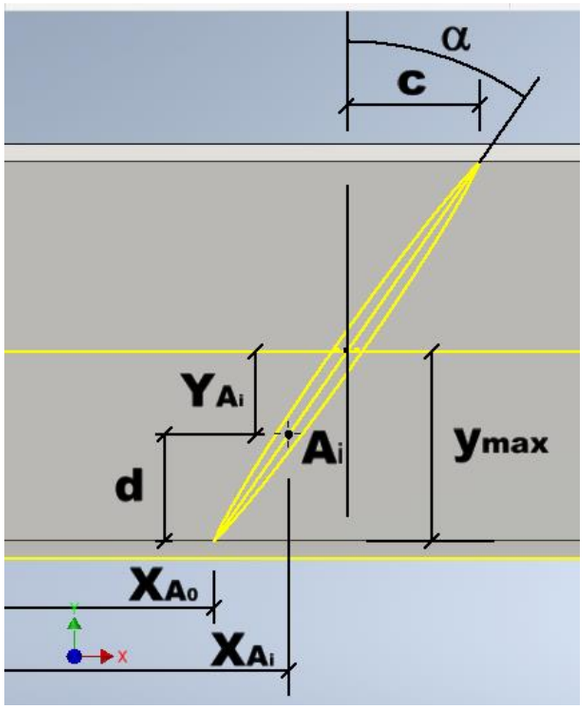

Figure 5 Detail of Figure 4
Source: Own elaboration

Figure 6 shows the tool in its path to generate the crack, from which the following equation can be inferred:

$$\overline{GH} = \frac{a}{sen(\alpha)} \quad (9)$$

ISSN 2414-4924

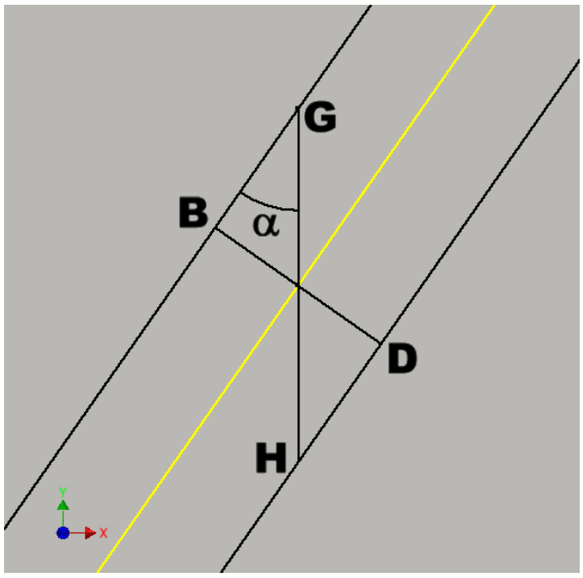

Figure 6 Tool and crack
Source: Own elaboration

Figures 7 and 8 show both the panoramic and detail view of a cross section of the rotor. Point Q is the intersection of the x-axis with the extension of the line segment MA_i. Point S is the intersection of the x-axis with the extension of the line segment NA_i. If we denote with **γ** half of the angle GA_iH as shown in Figure 8, the following equations are obtained from the afore mentioned Figures:

$$\frac{y_{NA_i}}{z_{NA_i}} = Tg(\gamma) = \frac{0.5\overline{GH}}{p} \quad (10)$$

$$y_{NA_i} = z_{NA_i} Tg(\gamma) \quad (11)$$

$$(y_N)^2 + (z_N)^2 = r^2 \quad (12)$$

$$\left[y_{A_i} + z_{NA_i} Tg(\gamma)\right]^2 + \left(z_{A_i} + z_{NA_i}\right)^2 = r^2 \quad (13)$$

(13) becomes (14), (15), (16) and (17); with the solution given by (18).

$$A\left(z_{NA_i}\right)^2 + Bz_{NA_i} + C = 0 \quad (14)$$

$$A = 1 + [Tg(\gamma)]^2 \quad (15)$$

$$B = 2y_{A_i} Tg(\gamma) + 2z_{A_i} \quad (16)$$

$$C = \left(y_{A_i}\right)^2 + \left(z_{A_i}\right)^2 - r^2 \quad (17)$$

$$z_{NA_i} = \frac{-B+\sqrt{B^2-4AC}}{2A} \quad (18)$$

Simultaneously the equation of the straight line through N and $A_i$with the equation of the z-axis yields.

$$z_S = \frac{Tg(\gamma) z_{A_i} - y_{A_i}}{Tg(\gamma)} \quad (19)$$

A similar procedure is used to obtain:

$$y_{MA_i} = -z_{MA_i} Tg(\gamma) \quad (20)$$

$$D = 1 + [Tg(\gamma)]^2 \quad (21)$$

$$E = 2z_{A_i} - 2y_{A_i} Tg(\gamma) \quad (22)$$

$$F = \left(y_{A_i}\right)^2 + \left(z_{A_i}\right)^2 - r^2 \quad (23)$$

$$z_{MA_i} = \frac{-E+\sqrt{E^2-4DF}}{2D} \quad (24)$$

$$z_Q = \frac{Tg(\gamma) z_{A_i} + y_{A_i}}{Tg(\gamma)} \quad (25)$$

Using the above equations we obtain:

$$\theta_{A_i} = Arc\ Tg\ \left(\frac{y_{A_i}}{z_{A_i}}\right) \quad (26)$$

$$z_N = z_{A_i} + z_{NA_i} \quad (27)$$

$$y_N = y_{A_i} + y_{NA_i} \quad (28)$$

$$\theta_N = Arc\ Tg\ \left(\frac{y_N}{z_N}\right) \quad (29)$$

$$z_M = z_{A_i} + z_{MA_i} \quad (30)$$

$$y_M = y_{A_i} + y_{MA_i} \quad (31)$$

$$\theta_M = Arc\ Tg\ \left(\frac{y_M}{z_M}\right) \quad (32)$$

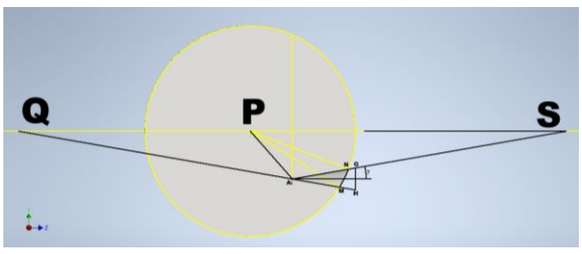

Figure 7 Cross section i=100
Source: Own elaboration

ISSN 2414-4924

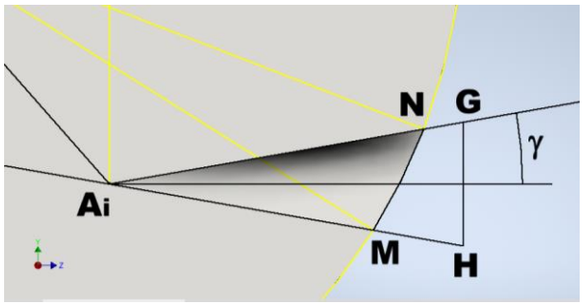

Figure 8 Detail of Figure 7
Source: Own elaboration

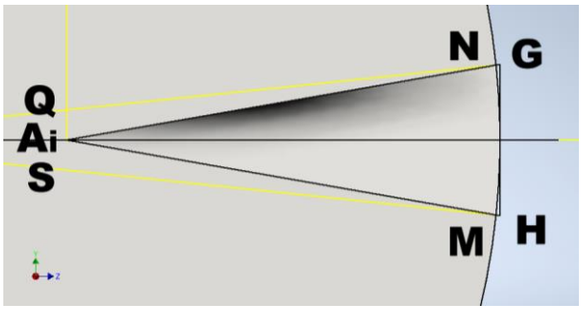

Figure 9 Cross section i=250
Source: Own elaboration

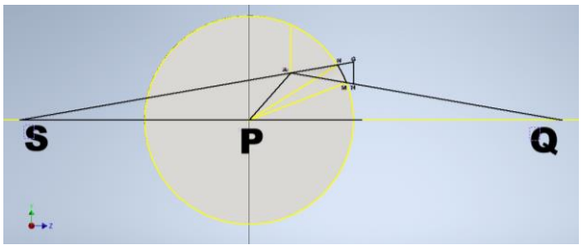

Figure 10 Cross section i=400
Source: Own elaboration

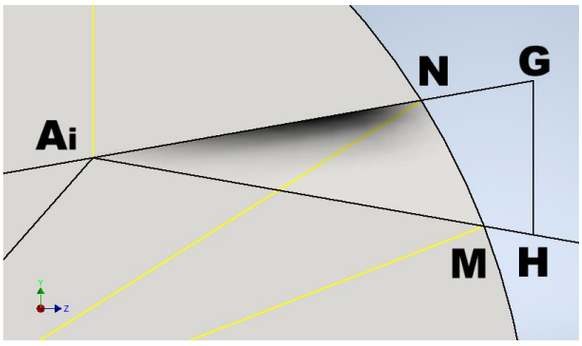

Figure 11 Detail of Figure 10
Source: Own elaboration

Component areas

Based on the two previous Figures and the three subsequent Figures, it is possible to define basic component areas of the complex area whose moment of inertia is of interest.

The area defined by the arc MN and by the line segments PN y PM is subtracted from the area of the circle defined by the circumference of radius r. Subsequently the areas PA_iN and PA_iM are added or subtracted.

For i varying from zero to 250 there are two possibilities:

- The angle $\theta_{A_i} \leq \theta_M$_M, the area PA_iN is to be added and the area PA_iM is to be subtracted.
- Angle $\theta_{A_i} > \theta_M$, area PA_iN must be added and area PA_iM must be added.

For i ranging from 251 to 500 there are two possibilities:

- The angle $\theta_{A_i} \leq \theta_N$, the area PA_iN must be summed and the area PA_iM must be summed.
- The angle $\theta_{A_i} > \theta_N$, the area PA_iN must be subtracted and the area PA_iM must be added.

The above component areas, in turn, are composite areas:

- $PA_iN = |PA_iS - PNS|$
- $PA_iM = |PMQ - PA_iQ|$

Moments of inertia of component areas

The moments of inertia of the component areas are as follows.

$$I_P = \frac{r^4}{8}[\theta_N - \theta_M + SC(\theta_M) - SC(\theta_N)] \quad (33)$$

$$SC(\theta_M) = sen(\theta_M)cos(\theta_M) \quad (34)$$

$$SC(\theta_N) = sen(\theta_N)cos(\theta_N) \quad (35)$$

$$I_{PA_iS} = \frac{|z_S|\left|y_{A_i}\right|^3}{12} \quad (36)$$

$$I_{PNS} = \frac{|z_S||y_N|^3}{12} \quad (37)$$

$$I_{PMQ} = \frac{|z_Q||y_M|^3}{12} \quad (38)$$

ISSN 2414-4924

$$I_{PA_iQ} = \frac{|z_Q||y_{A_i}|^3}{12} \quad (39)$$

$$I_{PA_iN} = |I_{PA_iS} - I_{PNS}| \quad (40)$$

$$I_{PA_iM} = |I_{PMQ} - I_{PA_iQ}| \quad (41)$$

Where I_P is the moment of inertia of the circular sector bounded by the arc MN and by the line segments PM, PN.

Moment of Inertia of the Area of Interest

The area whose moment of inertia is to be determined is shown in Figure 12.

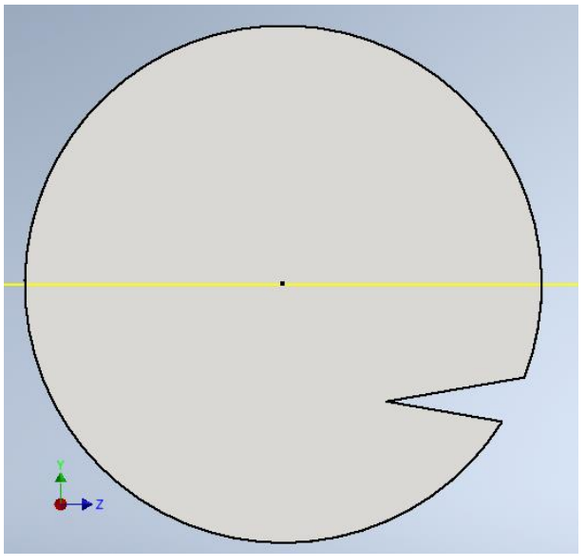

Figure 12 Area of interest
Source: Own elaboration

For i varying from zero to 250 and $\theta_{A_i} \leq \theta_M$:

$$I = I_c - I_P + I_{PA_iN} - I_{PA_iM} \quad (42)$$

For i varying from zero to 250 and $\theta_{A_i} > \theta_M$:

$$I = I_c - I_P + I_{PA_iN} + I_{PA_iM} \quad (43)$$

For i varying from 251 to 500 and $\theta_{A_i} \leq \theta_N$:

$$I = I_c - I_P + I_{PA_iN} + I_{PA_iM} \quad (44)$$

For i varying from 251 to 500 and $\theta_{A_i} > \theta_N$:

$$I = I_c - I_P - I_{PA_iN} + I_{PA_iM} \quad (45)$$

Where the subscript c refers to the complete circle.

Results

For a rotor of a specific machine whose operating regime does not change in years; the linear input parameters L and r, can be considered invariant; for similar reason such a rotor will be subjected to both torsion and bending and the ratio of the tangential stresses among the normal ones, being invariant, will imply a constant angle α.

The depth and width will increase steadily from birth and throughout the crack growth.

The previous two paragraphs justified the treatment to each of the input parameters.

For all $\boldsymbol{x_{A_i}}$, the following were determined:

- The coordinates (z, y) of A_i, N and M.
- The angles θ_{A_i}, θ_N y θ_M.
- Basic component areas (circle, circular sector and triangles).
- The moments of inertia of the areas of interest are shown in Figure 13 and complemented with Table 1.

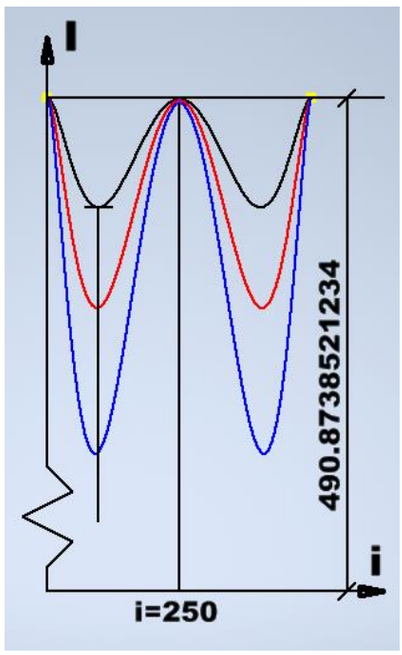

Figure 13 Moments of inertia
Source: Own elaboration

ISSN 2414-4924

Series	L	r	a	p	α
Black	100	5	0.4	2	1/6
Red	100	5	0.5	2.5	1/6
Blue	100	5	0.6	3	1/6

Table 1 Input parameters
Source: Own elaboration

Important relationships between the three series shown in Figure 13 can be seen in Figures 14 and 15.

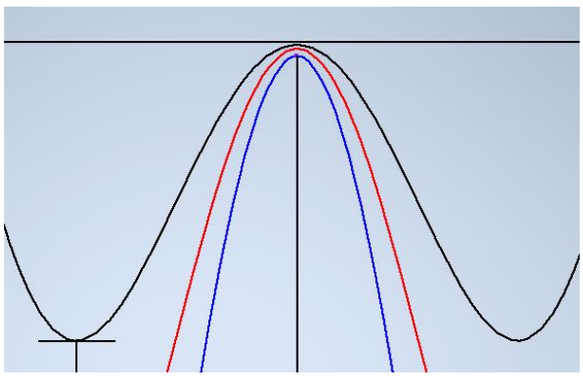

Figure 14 Detail Figure 13 i=250
Source: Own elaboration

In the center of the crack the moment of inertia decreases as we increase the depth, maintaining zero slope in the center of the crack.

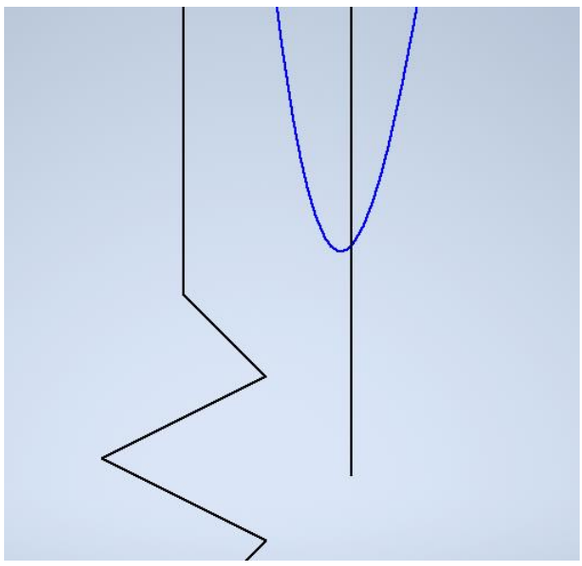

Figure 15 Detail Figure 13 lag
Source: Own elaboration

The vertical descending from the first minimum of the first series (black) passes slightly to the right of the first minimum of the third series (blue).

According to Figures 13, 14 and 15; Table 2 shows transcendent values of the presented series.

Series	I_{max}	I_{min}	I_{cf}
1	490.87	488.67	490.85
2	490.87	486.66	490.82
3	490.87	483.74	490.77

Table 2 Output parameters
Source: Own elaboration

Conclusions

The functional relationships presented allow to evaluate with accuracy and precision the moment of inertia of a rotor in all cross sections of its diagonal diagonal triangular chordal crack. Such relationships are applicable from the crack birth and during its growth; they constitute important elements of judgment in the early detection of cracks.

The results presented constitute an advance in the knowledge of the effect of a chordal diagonal triangular crack on the moment of inertia of a rotor. In this article the orientation of the crack was limited to the positive direction of the z-axis, in a later article it is convenient to evaluate the moment of inertia when the rotor is such and constantly modifies the orientation of the crack.

Acknowledgment

The authors are grateful for the institutional support of the Universidad Autónoma Metropolitana and the Unidad Azcapotzalco; in particular the logistic support of the Division of Basic Sciences and Engineering and the Department of Energy.

Funding

The present work has been funded by the Department of Energy [project EN001-22 EVALUATION OF THE EFFECT OF A CRACK IN THE ELASTIC BEHAVIOR OF A ROTOR].

ISSN 2414-4924

References

Lazarus, A. (2008). *Influence des dédauts sur le comportement vibratoire linéaire des systèmes tournants* (Tesis doctoral. Ecole doctorale de l'Ecole Polytechnique, Francia). Recuperado de http://www-cast3m.cea.fr/html/Theses_Cast3M/Lazarus.pdf

Ramezanpour, R., Ghayour, M. & Ziaei-Rad, S. (2012). Dynamic behavior of Jeffcott rotors with an arbitrary slant crack orientation on the shaft. *Applied and Conmputational Mechanics*, 6. Recuperado de https://pdfs.semanticscholar.org/21c3/0ebb28846d7dc29b2a5908c67a0e38d4d3ab.pdf?_ga=2.75022544.394348335.1584401537-1321827918.1583891375

Ghozlane, M. (2015). *Dynamic Response of Cracked Shaft in Rotor Bearing-Disk System*. Recuperado de: https://www.researchgate.net/publication/281890905_Dynamic_Response_of_Cracked_Shaft_in_Rotor_Bearing-Disk_System

Guo, G. & Liu, C. (2016). Stiffness Variation of a Cracked Rotor with a Semi-Elliptical Front. En *School of Mechanical and Power Engineering, East China University of Science and Technology, Shanghai, China en International Conference on Sustainable Energy, Environment and Information Engineering*. Bangkok, Tailandia.

Fellah, A., Hadjoui, A. & Bakhaled, B. (2017). Numerical Study of an Open Cracked Rotor. En *IS2M Laboratory,Faculty of technology, University of Tlemcen, Algeria de la International Conference on Mechanical, Aeronautical and Industrial Egineering*. Paris, Francia.

Bakhaled, B., Hadjoui, A. & Fellah, A. (2018). AN ALTERNATIVE WAY TO PREDICT THE PRESENCE OF CRACKS IN A ROTOR BY STUDYING ITS VIBRATIONAL BEHAVIOUR. *U.P.B. Scientific Bulletin,* 80. Recuperado de: https://www.scientificbulletin.upb.ro/rev_docs_arhiva/fullf72_29903.pdf

Jameel, A. & Thijeel, J. (2019). *Analytical Investigation of the Dynamics of Cracked Rotors* (Tesis doctoral. Baghdad University, Iraq). Recuperado de: https://www.researchgate.net/publication/330999316_Analytical_Investigation_of_the_Dynamics_of_Cracked_Rotors

Joseph, S. Helen, W. & Richard, Y. (2020). *Application of Non-Symmetric Bending Principles on Modelling Fatigue Crack Behaviour and Vibration of a Cracked Rotor*. Recuperado de: https://www.researchgate.net/publication/338731385_Application_of_Non-Symmetric_Bending_Principles_on_Modelling_Fatigue_Crack_Behaviour_and_Vibration_of_a_Cracked_Rotor

Peter, K. & Robert, G. (2021). *Measuring Mass Moment of Inertia of a Rotor-Two Simple Methods Using no Special Equipment*. Recuperado de: https://www.researchgate.net/publication/337990159_Measuring_Mass_Moment_of_Inertia_of_a_Rotor-Two_Simple_Methods_Using_no_Special_Equipment

Mohammad, A. & Fatima, K. (2021). *Negative potential energy content analysis in cracked rotors whirl response*. Recuperado de: https://www.ncbi.nlm.nih.gov/pmc/articles/PMC8316492/

Mo, Y. Hao, X, & Wei, X. (2022). *Analytical bending stiffness model of composite shaft with breathing fatigue crack*. Recuperado de: https://www.researchgate.net/publication/361638451_Analytical_bending_stiffness_model_of_composite_shaft_with_breathing_fatigue_crack

ISSN 2414-4924